Neutrophil extracellular traps impair regeneration.

Authors:
Eric Wier[1], Mayumi Asada[1], Gaofeng Wang[1,2], Martin P. Alphonse[1], Ang Li[1], Chase Hintelmann[1], Christine Youn[1], Brittany Pielstick[3], Roger Ortines[1], Lloyd S. Miller[1,4], Nathan K. Archer[1], Luis A. Garza[1]

Affiliations:
[1]Department of Dermatology, Johns Hopkins University School of Medicine, Baltimore, Maryland, USA.

[2]Department of Plastic and Aesthetic Surgery, Nanfang Hospital of Southern Medical University, Guangzhou, Guangdong Province, China.

[3]Department of Molecular Biology and Genetics, Johns Hopkins University, Baltimore, Maryland, USA.

[4]Immunology, Janssen Research and Development, 1400 McKean Road, Spring House, PA, 19477, USA (Current affiliation. All work performed at prior affiliation[1])

* Correspondence to: LAG@jhmi.edu

Abstract
Fibrosis is a major health burden across diseases and organs. To remedy this, we study wound induced hair follicle regeneration (WIHN) as a model of non-fibrotic healing that recapitulates embryogenesis for de novo hair follicle morphogenesis after wounding. We have previously demonstrated that TLR3 promotes WIHN through binding dsRNA, but the source of which is still unclear. Here, we demonstrate that multiple distinct contexts of high WIHN all show a strong neutrophil signature, and given the likelihood of nuclear dsRNA release during the production of neutrophil extracellular trap (NETs), we hypothesized that mature neutrophils and NETs might promote WIHN. Consistent with this, in addition to the presence of mature neutrophils shortly after wounding, neutrophils remain within the wound after the barrier is reestablished, where they produce extracellular traps (NETs) that likely release spliceosomal U1 dsRNA. Contrary to our hypothesis, genetic models of neutrophil depletion show enhanced WIHN. Pad4 null mice that are defective in NET production also augment WIHN. Finally, using single-cell RNA sequencing, we identified a dramatic increase in mature neutrophils in the wound beds of low regenerating Tlr3-/- mice. Taken together, these results demonstrate that although mature neutrophils are stimulated by a common pro-regenerative cue, their presence and NETs hinder WIHN.

Introduction

After suffering a wound, the body initiates a well-coordinated physiological process to restore homeostasis and reestablish the barrier. This spontaneous process comprises four

discrete phases: hemostasis, inflammation, proliferation, and remodeling[1]. Although all of these phases have been extensively studied, the molecular details as to why repair tends to result in fibrotic scar tissue rather than complete regeneration have not been fully elucidated. This tendency of wound repair to lead to fibrosis, and in some cases, hypertrophic scars, contributes an enormous burden on human health[1-3]. Inflammation and different components of the immune system have been shown to contribute to regeneration in salamanders and zebrafish, as well as to promote healing and maintain barrier function in mammals upon mucosal injury[4-6]. Although the cellular effects of macrophages and T cells are well studied[7-10] , the role of neutrophils in modulating regeneration remains elusive.

Unlike urodele salamanders, complete skin regeneration after wounding in mammals is rare[11]. It occurs via de novo hair follicle generation in mice and rabbits through a process that mimics skin embryogenesis[12-15]. This process of de novo follicle neogenesis (Wound Induced Hair Neogenesis; WIHN) was first fully characterized in mice after receiving full thickness wounds[16]. These regenerated follicles establish a distinct stem cell population, express characteristic differentiation markers, produce functional hair shafts, and can complete the hair cycle. In addition to the hair follicles, sebaceous glands, specialized vascular and nerve supports, and surrounding fat cells are regenerated[16,17].

Immediately after wounding, a robust inflammatory phase occurs, which allows the ingress of keratinocytes and fibroblasts to proceed afterward. The early stage of wound healing is defined by the dramatic recruitment of mature neutrophils, which are instrumental in providing defense against microbial pathogens[18-22]. This is followed by an influx of macrophages (Mϕ's) that continue the phagocytic processes begun by neutrophils and aid in the transition to the proliferative phase of wound healing[23-25]. While much is known about the importance of this inflammatory phase for preventing and abrogating infections, less is known about how it influences regenerative capacity or WIHN. Increasingly, macrophages have been shown to be essential for WIHN via TNF-induced AKT/ β-catenin signaling[8-10]. However, the role of neutrophils in modeling regeneration or WIHN is unclear.

Toll-like receptors (TLRs) are highly conserved single-pass membrane-spanning receptors that recognize structurally conserved molecular components of invading microbes and activate a cascade of inflammatory signaling pathways[26]. Rather than simply recognizing pathogen associated molecules, they can also initiate "sterile" inflammation upon recognizing damage-associated molecular patterns (DAMPs), which are critical to recruit immune cells and initiate wound healing[27]. TLR3 is activated by dsRNA and has primarily been studied in the context of viral infection[28]. Mounting evidence shows that TLR3 also plays an important role in wound repair[29-37]. Synthetic double strand RNA (dsRNA) polyriboinosinic-polyribocytidylic acid (poly(I:C)) treatment dramatically increases WIHN in mice. Furthermore, wound-released dsRNA activates TLR3 to promote hair follicle regeneration[34]. The identity and source of the physiological RNA remains an open and important question in the field. Notably, the dsRNA U1 spliceosomal small nuclear RNA (snRNA), may be an important endogenous RNA sensed via TLR3[32,33,38,39]. Specifically, UV damage releases U1 snRNA that stimulates cytokine production in keratinocytes and increases barrier gene transcription[32,33].

In addition to phagocytosis and degranulation, mature neutrophils can produce extracellular traps (ET), large extracellular web-like structures composed of decondensed chromatin bound to various cytosolic and granule proteins[21,22,40-42]. While originally recognized

as a defense mechanism against pathogens[21,40,41], they have also been found to mediate sterile inflammatory processes[43,44]. In the absence of infection, ETs can be stimulated in sterile tissue environments through various cytokines[41,45-47] and by activated platelets[43,44]. Interestingly, ETs are found within sterile wounds of mice and delay wound healing[48]. Mechanistically, ETs are formed by the rapid decondensation of the cellular chromatin, followed by the fragmentation of the nuclear membrane and mixing of the nuclear and cytoplasmic compartments, before being expelled from the cell. The ability of neutrophils to rapidly migrate to the wound site and produce ETs, coupled with the nuclear localization of some dsRNA, made us question whether neutrophils were a source of the dsRNA critical for WIHN. Interestingly, while there are extensive studies on the DNA components released during ET formation[22,42,49], the RNA components are poorly understood.

To probe how mature neutrophils influence wound regeneration and WIHN, we analyzed multiple microarrays from distinct contexts of high regenerating mice and found a common neutrophil signature. Using immunofluorescence and flow cytometry we found that neutrophils remain in the wound bed, albeit at low levels, after the acute inflammatory phase, where they produce NETs that contain the nuclear U1 dsRNA. To define how this influences regeneration, we used antibody mediated neutrophil depletion to eliminate neutrophils from the wound bed at select time points, but discovered that the technique is ineffective in the context of large full-thickness wounds, which are necessary to initiate WIHN. However, using a neutrophil-specific diphtheria toxin ablation model, we were able to deplete mature neutrophils in the wound bed and found that—contrary to our initial hypothesis-- the absence of mature neutrophils enhances WIHN. Eliminating neutrophil's ability to produce NETs by knocking out Pad4 also boosted WIHN, confirming the negative influence of neutrophils on regeneration. Finally, we used single-cell RNA sequencing to characterized WIHN deficient Tlr3-/- mice and found that they have a dramatically increased population of mature neutrophils in the re-epithelized wound bed, compared to wild-type mice, likely contributing to their diminished regenerative capacity. These results indicate that, while important for preventing infection, mature neutrophils and their NETs negatively impact regeneration and WIHN. Although a common pro-regenerative signal might increase neutrophil infiltration, mature neutrophils instead likely contribute to fibrosis.

Results

Neutrophil signature present during skin regeneration

To begin to characterize the role of neutrophils in WIHN, we performed bioinformatic analysis on previous microarrays of multiple distinct high regenerating mouse models, probing for innate immune and neutrophil signatures. First, we analyzed the proteome comparing the center of the re-epithelialized wound bed (high WIHN) to the surrounding periphery/edge (low WIHN) (Fig. 1a)[37]. Gene ontology analysis revealed that, in the area of high WIHN, neutrophil aggregation and other defense pathways against bacterium are enriched, characterized by an abundance of antimicrobial and granular proteins, such as Neutrophil Elastase (Elane), Cathelicidin (Camp), and Myeloperoxidase (Mpo) (Fig. 1b-c). In a second model system, high WIHN Rnasel-/- mice (manuscript in review), at the time of scab detachment, are also enriched

129 in genes associated with neutrophils. Neutrophil chemotaxis is the most significant upregulated
130 gene ontology category, with other chemotactic and inflammatory pathways up as well (Fig.
131 1d). Finally, we analyzed the gene expression changes between wounded specific pathogen free
132 (SPF) mice, which have increased regeneration and WIHN, when compared to germ free (GF)
133 mice (manuscript in review), at the time of scab detachment. Like the other two high
134 regeneration models, when compared to GF, SPF mice had elevated neutrophil chemotaxis and
135 immune response transcripts (Fig. 1e). Together, these disparate experimental contexts
136 demonstrate that neutrophil chemotaxis can correlate with high regeneration and WIHN.
137
138 **Neutrophils persist in the wound bed after the acute inflammatory phase, producing**
139 **extracellular traps**
140
141 Given the above correlations of high neutrophil infiltration to high WIHN, we first
142 characterized mature neutrophil infiltration in the wound beds of C57BL/6J mice after a large
143 square wound cut into the center of their backs, to the depth of fascia. As anticipated,
144 neutrophils are abundant in the acute phase of the wound healing process (1-3 days post
145 wounding), as seen by H&E staining (Fig. 2a) and immunofluorescence of Myeloperoxidase
146 (MPO), a major neutrophil granule protein (Fig. 2b). While neutrophils predominate at early
147 time points, they are still present in the wound bed as late as wound day 11, well after re-
148 epithelization has completed (Fig. 2c). In contrast, macrophages only accumulate starting at
149 wound day 3 (Fig. 2b) but remain a major component of the wound even after re-epithelization
150 (Fig. S1). These results show the dynamic changes of immune cell infiltration, but with an
151 underappreciated persistence of some neutrophils late in wound healing, during the time of
152 morphogenesis.
153 Given the importance of dsRNA to promote WIHN, and the association of neutrophils
154 with high WIHN, we hypothesized that neutrophil extracellular traps (NETs) release of
155 neutrophil nuclear content might release dsRNA, in addition to dsDNA, from the nucleus to
156 promote WIHN. We visualized citrullinated histone H3 (H3Cit) to identify NETS as early as
157 wound day 3 (Fig. 2d). The production of NETs is mediated by Pad4, an enzyme that modifies
158 the arginine residues on histones to citrulline, which changes their charge, leading to massive
159 chromatin decondensation[50,51]. Consistent with this, NETs are virtually absent in mice lacking
160 Pad4, while abundant in the wound bed after the acute phase of wound healing in WT mice
161 (Fig. 2e). Although NETs are characterized by their extruded DNA, which forms a web-like
162 scaffold containing cytosolic and granular proteins, little is known about the RNA content within
163 them and how that might influence wound healing. Given that U1 small nuclear (sn) RNA is
164 proposed as a TLR3 agonist damage-associated molecular pattern important for skin barrier
165 repair[32,33], we visualized it by FISH. U1 snRNA is present throughout the wound beds of
166 C57BL/6J mice (Fig. 2f). Rather than the baseline nuclear appearance of unwounded tissue, U1
167 snRNA in the wound bed is markedly cytoplasmic, suggesting that its cellular localizations shifts
168 from the nucleus as a potential step towards cellular release. Consistent with this, we noted a
169 fine haze of signal extracellularly. Taken together, these data suggest a potential model where
170 neutrophils persist to the morphogenesis stage of wound healing and release extracellular traps
171 that contain U1 dsRNA to perhaps modulate WIHN.
172

173
174 **Large full-thickness wounds dramatically reduce antibody-mediated neutrophil depletion**
175
176 To functionally assess how neutrophils modulate wound induced hair neogenesis
177 (WIHN), we sought to deplete neutrophils throughout the wound bed at select times. To
178 accomplish this, we adapted a widely used antibody mediated depletion scheme, where we
179 injected neutrophil specific antibodies intraperitoneally (Fig. 3a)[52]. Most experiments were
180 completed using a Ly6G positive monoclonal antibody (1A8 clone), which recognizes a 21-25kD
181 glycosylphosphatidylinositol (GPI)-linked differentiation antigen that is expressed by myeloid-
182 derived cells. While monocytes transiently express Ly6G during bone marrow development,
183 Ly6G expression in peripheral neutrophils directly correlates its level of differentiation and
184 maturation. The less specific anti-granulocyte receptor-1 (Gr-1) antibody (RB6-8C5 clone),
185 which recognizes both Ly6G and Ly6C and thereby also targets dendritic cells and
186 subpopulations of lymphocytes and monocytes, was also used in select experiments. To
187 prevent confounding flow cytometry measurements caused by epitope masking from the initial
188 Ly6G antibody injected during the antibody mediated neutrophil depletion experiments[53], a
189 distinct Ly6G antibody clone was used for analysis via flow cytometry. Injections were done one
190 day before and one day after large full-thickness wounds on the back of mice. The depletion
191 scheme focused on the early time points of the wound healing process because those were
192 shown to be most critical in dsRNA-Tlr3 enhanced WIHN[34].
193 Unexpectedly, on wound day 3, after receiving two IP injections of either Ly6G or Gr-1
194 antibodies, using our careful detection strategy, there was no apparent neutrophil depletion in
195 the wound bed, as measured via flow cytometry (Fig. 3b). Depletion was also ineffective in
196 other tissues after wounding, including the spleen and liver (Fig. S3). Looking one day earlier
197 (wound day 2), neutrophil depletion was still ineffective in the wound bed, but there was a
198 statistically significant depletion in the blood of the same mice (Fig. 3c). Although significant,
199 the neutrophil depletion was less than 50%, far less efficient than the previous reports[52,54,55].
200 An important distinction between ours and previous work is that we employed depletion in the
201 context of large wounds to fascia, prompting us to question whether large area wounding
202 globally modifies neutrophil blood trafficking dynamics to result in depletion failure. Indeed,
203 neutrophil depletion was very efficient in the blood of unwounded mice who had received an IP
204 injection of the Ly6G (1A8 clone) antibody 24 hours earlier (Fig. 3d), but this depletion was
205 abolished after wounding the mice (Fig. 3e). To explore this further, we repeated the injection
206 scheme in Fig. 3a. With and without wounding mice, we examined the neutrophil depletion in
207 the blood and wound bed at wound day 2. Consistent with our previous experiments, in the
208 context of wounding, the Ly6G (1A8) neutralizing antibody achieved less than 50 percent
209 neutrophil depletion in the blood. In contrast, mice that were not wounded, achieved
210 substantially more efficient depletion in the blood (Fig. 3f). Unwounded skin does not typically
211 contain neutrophils, so the Ly6G (1A8 clone) antibody injection had no effect (Fig. 3g).
212 Wounding caused dramatic recruitment of neutrophils to the wound bed, as shown earlier (Fig
213 3b-c, e). Ly6G antibody injection could not overcome this to deplete neutrophils from the
214 wound bed (Fig. 3g).
215 A previous report had success with antibody-mediated neutrophil depletion in a
216 wounding model where small 2cm excisions were made[55], leading us to question whether Ly6G

217 (1A8 clone) antibody injection was more effective in smaller, full-thickness wounds. To address
218 this, mice were injected with Ly6G (1A8 clone) antibody and then wounded with large wounds
219 (1.25x1.25cm2), like the previous experiments, or smaller wounds (0.6x0.6cm2) (Fig. 3h).
220 Neutrophil depletion efficacy was then assessed at wound day two in the blood and wound
221 bed. Mice that had been given small wounds had significant neutrophil depletion in both the
222 blood and wound bed, while those with the large wounds did not (Fig 3i-j). Taken together,
223 these data suggest that antibody mediated neutrophil depletion, while efficient in certain non-
224 wounding contexts, is not effective after the large full-thickness wounds necessary to induce
225 WIHN—perhaps because of the unusually robust stimuli of neutrophil recruitment in this
226 context.
227
228 **Mature Neutrophils inhibit wound induced hair neogenesis**
229
230 Despite the minimal inhibition of neutrophils using conventional antibody depletion
231 with large wounds, we sought to begin testing how neutrophils might modulate WIHN. We
232 used the same antibody depletion scheme described (Fig 3a) but allowed the mice to recover
233 for 21 days before quantifying WIHN via confocal scanning laser microscopy (CSLM) (Fig 4a)[56].
234 Antibody injection did not affect wound closure speed (Fig. S4). Despite minimal neutrophil
235 depletion within the wound beds of mice post Ly6G (1A8 clone) injection (Fig 3b, c, e, g), the
236 number of regenerated hair follicles was increased, suggesting that neutrophils may hinder
237 WIHN (fold = 3.94) (Fig 4b).
238 To surmount the difficulties with meager neutrophil depletion using Ly6G antibodies,
239 we generated a transgenic mouse model for selective and inducible ablation of neutrophils
240 upon injection of diphtheria toxin (DT)[57]. MRP8-Cre mice expressing Cre recombinase under the
241 control of the neutrophil-associated human MRP8 promoter[58-60] were crossed with ROSA-iDTR^{KI}
242 mice, which have a Cre-inducible simian DT receptor (DTR)[61]. This generated mice with DTR
243 expression restricted to mature neutrophils that suffer cell death selectively after the injection
244 of DT. Two injections, one before wounding and one a day after, had no effect on control mice
245 (PMN^{WT} mice: MRP8-Cre−, ROSA-iDTR^{KI}) but substantially reduced neutrophil numbers in the
246 blood (fold = -4.33) and wound beds (fold = -4.27) of PMN^{DTR} (MRP8-Cre+, ROSA-iDTR^{KI}) mice at
247 wound day 2 (Fig. 4c-d). We next followed the mice after neutrophil ablation in the early phase
248 of wounding to find WIHN was substantially elevated (fold = 3.23) (Fig. 4e). The ablation of
249 neutrophils later in the wound healing process yielded the same results (Wound days 6, 8, and
250 10) (Fig. S5). Antibody mediated depletion (1A8 clone) at these later time points had no effect
251 on WIHN, suggesting that although effective in the blood, it is not able to target neutrophils
252 already present within the wound bed (Fig. S6). After overcoming the technical hurdles above,
253 these data suggest that neutrophils have a detrimental effect on the regeneration of hair
254 follicles.
255 To further explore this possibility, we sought to try a gain-of-function approach, rather
256 than the loss-of-function approach above. We injected purified neutrophils from the bone
257 marrow of mice into the wound beds of mice during the re-epithelialization process. Although
258 not significant, likely due to the high variability of WIHN, the addition of 200,000 neutrophils
259 reduced the number of regenerated hair follicles (fold = -0.73) (Fig. 4f).

Finally, given the presence of NETs late in wound healing (Fig 2e), we sought to test the role of NETs in hair follicle neogenesis directly. We, therefore, tested WIHN in NET-deficient Pad4 KO mice, as employed in Figure 2e. In the absence of Pad4 and with dramatically reduced NETs, WIHN is enhanced (fold = 2.47, p = 0.026) (Fig. 4g). This suggests that NETs play a role in reducing the regenerative capacity of mice during the wound healing process. This correlates with the capacity of NETs to damage tissue in diseases such as small vessel vasculitis[62], systemic lupus erythematosus[63-67], rheumatoid arthritis[68], and psoriasis[69].

Single-cell RNAseq correlation of mature neutrophils with poor WIHN

Double-stranded RNA sensing, mediated by Tlr3 and downstream effector pathways Il-6/ Stat3, has been shown to be critical for WIHN, with Tlr3-/- mice having substantially less regenerated hair follicles than their wild-type controls[34]. Given that TLR3 dsRNA sensing has been shown to be critical for neutrophil recruitment and NET production in a model for acute lung injury (ALI) and glomerulonephritis (GN), we wondered if Tlr3-/- mice paradoxically have increased neutrophil levels, contributing to lower WIHN[70,71]. As anticipated, Tlr3-/- mice had substantially less WIHN than their WT controls (fold = -3.75, p = 0.0218) (Fig. 4h, Fig. S7a). We performed single-cell RNA sequencing on wildtype and Tlr3-/- re-epithelialized wound beds of mice 10 days post wounding and prior to morphogenesis. Approximately 8014 sequenced cells met standard quality control metrics and were further analyzed in the Seurat R package[72]. Unsupervised clustering and UMAP non-linear dimensional reduction identified 18 cell clusters. Seurat generated conserved and differentially expressed genes to assign cluster identities. We found the mature neutrophil cluster to be substantially increased in the Tlr3-/- mice (Fig. 4i, Fig. S7b). This disparity is evident when looking at select differentially expressed neutrophil associated genes that are all elevated in Tlr3 -/- mice (Fig. 4j). Together, these data suggest that elevated mature neutrophil levels within Tlr3-/- mice correlate with their deficiency in WIHN.

Discussion

The wound healing process is a careful balance of interconnected steps that must weigh the benefits of quick barrier repair, which leads to fibrous scarring, and more complete regeneration, that restores function and appearance. The role inflammation plays in regeneration and scarring is still being elucidated, but increasing evidence suggests that neither excess nor lack of inflammation supports regeneration. Fgf9-producing γ-δ T cells are critical for WIHN, infiltrating into wound bed immediately before re-epithelialization and onset of hair follicle regeneration[7]. Macrophages have also been shown to be important in the process, with their ablation eliminating WIHN[8-10]. Additionally, the injection of the dsRNA mimic poly(I:C), as early as 3 days after wound, dramatically enhances WIHN[34]. Intriguingly, spiny mice (*Acomys*) have a dramatically reduced inflammatory response post wounding, with less cytokines and virtually no macrophages until late in the process, when compared to laboratory mice (*Mus*), despite having substantially improved regeneration[73,74]. Consistent with this idea of a complex network of inflammatory cells influencing regeneration, we show that neutrophils persist in the

299 wound bed after the acute inflammatory phase and—despite multiple correlations to the
300 contrary-- have a detrimental effect on regeneration.

301 Using histological and flow cytometry techniques, we show that while abundant
302 immediately after wounding, mature neutrophils remain in low levels within the wound bed
303 after re-epithelization. These late stage neutrophils produce NETs, which are eliminated in mice
304 that are deficient in Pad4, an enzyme critical for chromatin decondensation and NET
305 formation[50,51]. Critically, Pad4-/- mice have increased WIHN, when compared with WT mice.
306 Furthermore, antibody mediated and selective genetic neutrophil ablation dramatically boost
307 WIHN. Single-cell RNA sequencing also revealed that mice deficient in dsRNA sensing Tlr3, who
308 have severely reduced WIHN, have substantially more mature neutrophils present in the re-
309 epithelized wound bed, immediately preceding regeneration. All these data suggest a model
310 where neutrophils play an important role in defense against bacterial pathogens, but if they
311 persist within the wound bed too long after barrier repair, regeneration is hindered. In the
312 future, it will be interesting to see if selectively targeting NETs (e.g., PAD4 inhibitors, DNase I, N-
313 acetylcysteine) enhance regenerative wound repair.

314 When attempting to deplete neutrophils to assess their effects on WIHN, we also
315 discovered that the commonly used antibody depletion methods were not effective. Two
316 neutrophil-specific antibodies, which recognize different epitopes of the GPI-linked
317 differentiation antigen Ly6G, are commonly injected to rapidly deplete circulating neutrophils.
318 The most widely used clone (1A8) specifically recognizes Ly6G, while the anti-granulocyte
319 receptor-1 (Gr-1) antibody (RB6-8C5 clone) recognizes a heterodimer of Ly6G and Ly6C, making
320 it partially target monocytes. Both antibodies efficiently depleted neutrophils in unwounded
321 animals. When large full-thickness wounds (1.25x1.25cm^2) were used, which are necessary to
322 initiate WIHN, depletion levels in the blood were drastically reduced, while having negligible
323 effects on neutrophils within the wound bed. Depletion efficacy was restored if smaller wounds
324 were used (0.6x0.6cm^2), albeit at reduced levels when compared to unwounded mice. These
325 results suggest that wounding has a dramatic effect on recruiting neutrophil precursors for
326 mobilization and release, overwhelming the standard ability of depletion antibodies to work
327 effectively. This highlights the importance of rigorously testing antibody mediated depletion
328 methods in mouse models, to ensure they are achieving appreciable depletion. Furthermore, it
329 is important to carefully design neutrophil detection methods to assess depletion efficacy,
330 particularly with flow cytometry. Robust depletion can be erroneously detected if similar Ly6G
331 clones are used for both depletion and detection, due to epitope masking[53]. This can occur
332 since identical monoclonal clones are sometimes given different clone numbers. Antibody
333 manufacturers are increasingly manipulating antibodies to reduce undesirable features like
334 non-specific binding, without affecting the epitope-binding variable region, yet renaming the
335 clones, necessitating substantial effort to ensure non-overlapping epitope binding by both
336 depletion and analytical flow antibodies.

337 Our work generates important areas of future investigation. One question is unraveling
338 the paradox of why neutrophil infiltration signatures correlate with high WIHN, but mature
339 neutrophils inhibit WIHN. One possible model is that a common upstream cue or factor both
340 promotes WIHN and promotes neutrophil infiltration, but the latter serves to limit WIHN in
341 favor of decreasing infection risk. Defining this common upstream signal will be important for

342 future work. It will also be interesting to define the function of neutrophils within the re-
343 epithelized wound since the barrier has been restored. Another important question is whether
344 nuclear RNAs released in NETs have any function besides the general theorized one for released
345 DNA. Though NETs inhibit WIHN, nuclear RNA release in NETs might have functions in separate
346 physiological processes that will yield important insights. A final question is the identity of the
347 neutrophil mobilization factor whose strength correlates to wound size. Potential signals
348 include products of complement activation (C5a) or a number of small molecular weight C-X-C
349 chemokines, which are recognized by Cxcr1 and Cxcr2[75,76].

350 In summary, we here demonstrate a novel role for NETs and mature neutrophils to
351 inhibit regeneration. Future studies will be important to further understand the biology of
352 regeneration and test the capacity for neutrophil inhibition to promote regenerative healing.

353

354 **Acknowledgments:** The authors also thank Conover Talbot Jr. (JHMI Deep Sequencing and
355 Microarray Core) for assistance with microarray analysis.

356

357 **Competing financial interests:** L.S.M. is a full-time employee of Janssen Pharmaceuticals and
358 may hold Johnson & Johnson stock and stock options. L.S.M. performed all work at his prior
359 affiliation at Johns Hopkins University School of Medicine and he has received prior grant
360 support from AstraZeneca, Pfizer, Boehringer Ingelheim, Regeneron Pharmaceuticals, and
361 Moderna Therapeutics, was a paid consultant for Armirall and Janssen Research and
362 Development, was on the scientific advisory board of Integrated Biotherapeutics and is a
363 shareholder of Noveome Biotherapeutics, which are all developing therapeutics against
364 infections and/or inflammatory conditions.

365

366 **Funding:** Research reported in this publication was supported by the National Institute of
367 Arthritis, Musculoskeletal, and Skin Diseases, part of the National Institutes of Health, under
368 1F32AR074865-01 to EW and R01AR064297/AR068280 to LAG.

369

370 **Methods**

371 *Mouse Lines*

372 All wild-type and control mice used for in vivo experiments were on the C57BL/6J background.
373 All mice were age-matched and co-housed until 3-weeks of age. *Pad4* knockout mice were
374 purchased from the Jackson Laboratory (B6.Cg-Padi4$^{tm1.1Kmow}$/J, 030315). The diphtheria toxin
375 (DT) mediated neutrophil ablative mice were generated by crossing ROSA26iDTR (C57BL/6-
376 Gt(ROSA)26Sor$^{tm1(HBEGF)Awai}$/J , 007900) and MRP8-Cre-ires/GFP (B6.Cg-Tg(S100A8-cre,-
377 EGFP)1Ilw/J, 021614) from the Jackson Laboratory to get heterogeneous mice and genotyped
378 according to their specifications. Mice who genotyped positive for Cre (MRP8-Cre+; ROSA-
379 iDTR^{KI}) were considered PMN^{DTR} mice, while those that were negative for Cre (MRP8- Cre−;
380 ROSA-iDTR^{KI}) were PMN^{WT} littermate controls[57]. Tlr3 knockout mice (B6N.129S1-Tlr3^{tm1Flv}/J,

009675) and C57BL/6NJ controls (005304) were purchased from the Jackson Laboratory. All mice were bred and housed at an American Association for the Accreditation of Laboratory Animal Care (AAALAC)-compliant facility, and all experimental procedures were reviewed and approved by the Johns Hopkins University Institutional Animal Care and Use Committee (IACUC).

Wound Induced Hair Neogenesis (WIHN) Assay

All in vivo experimental surgical procedures were performed as previously characterized[7,16,34,37,77]. Briefly, after exposure to anesthesia (Baxter, Isoflurane), the dorsal side of 3-week-old (21 days) male and female mice were shaved. Surgical scissors were used to excise 1.25x1.25cm^2 of skin, creating wounds deep into the fascia. Approximately 3 weeks after wounding (~21 days), neogenic hair follicles in the re-epithelialized skin tissue were quantified using reflectance confocal scanning laser microscopy (CSLM) as previously published[34,37].

Neutrophil Depletion

C57BL/6J mice were depleted with 100 or 500µg of anti-Ly6G (Bio-X-Cell, 1A8 clone, BP0075-1) via intraperitoneal injection (IP) injection one day prior to and one day after wounding mice[52,54]. Select experiments also used 200µg of anti-Gr1 (Bio-X-Cell, RB6-8C5 clone, BP0075). LgG2a (Bio-X-Cell, BE0089) and IgG2b (Bio-X-Cell, BP0090) isotype controls were used for Ly6G or Gr1 experiments, respectively. DT depletion was done with PMN^{DTR} and PMN^{WT} littermate control mice that were IP injected with 250ng DT (Sigma-Aldrich). The injections were primarily done one day before and after wounding, or at wound days 6, 8, and 10.

Flow Cytometry

Flow cytometry was used to access neutrophil depletion. Blood was collected via retro-orbital sinus bleeds, and red blood cells were lysed RBC lysis buffer (BioLegend, 420301). Wound beds were surgically removed, and cell suspensions were prepared by digesting the tissue in a cocktail consisting of Liberase TL (Roche, 5401020001) and DNase I (Sigma, DN25) in RPMI 1640 (Gibco, 11875093). Cells were washed and then Fc blocked (BioLegend, 101320), before staining with an antibody cocktail (Extended Table 1). Finally, cells were washed and resuspended in FACs buffer containing Propidium Iodide (Miltenyi, 130-093-233). All flow cytometry experiments were performed on a BD LSR II, and downstream analysis of data was performed using FlowJo.

Neutrophil Extracellular Trap measurement

Wound beds were surgically removed at wound days 2 and 7, using a 6mm biopsy punch to remove excess tissue. Cell suspensions were prepared by digesting the tissue in a cocktail consisting of Liberase TL (Roche, 5401020001) and DNase I (Sigma, DN25) in RPMI 1640 (Gibco, 11875093). Cells were washed, and then Fc blocked (BioLegend, 101320), before staining with an antibody cocktail containing anti-MPO (Abcam, ab208670, 1:500) or respective isotype control (Abcam, ab172730, 1:500). Cells were then stained with a secondary Alexa Fluor 647 antibody (Abcam, ab150083, 1:2000). On the final wash, SYTOX green was added (ThermoFisher, S7020, 1:1000). This was performed on a BD LSR II, and downstream analysis of data was performed using FlowJo.

425
426 *3'-end single-cell RNA-sequencing:*
427 The re-epithelialized wounds beds (wound day 10) of a Tlr3-/- and a C57BL/6NJ control mouse
428 were excised, and cell suspensions were prepared by digesting the mouse skin tissue in a
429 cocktail consisting of Liberase TL (Roche, 5401020001) and DNase I (Sigma, DN25) in RPMI 1640
430 (Gibco, 11875093). Propidium iodide and DAPI positive dead cells were removed via cell sorting
431 with a BD FACSAria II. Single-cell libraries were prepared via a 10× Genomics Chromium Single-
432 Cell Platform, followed by sequencing using Illumina NovaSeq 6000. The results were run
433 through Cell Ranger pipeline software for sequence alignment and basic filtering. GEM
434 generation, barcoding, cDNA amplification, library preparation, quality control, and sequencing
435 were performed at the Genomics High Throughput Sequencing facility at Johns Hopkins School
436 of Medicine.
437
438 Downstream analysis, after the Cell Ranger pipeline, was done using the Seurat R package. A
439 standard pre-processing workflow was done, removing low quality cells or doublets, filtering
440 unique feature count over 3750 and below 200, as well as filtering out cells with higher than 5%
441 mitochondrial counts. This resulted in 4150 WT and 5648 Tlr3-/- cells for downstream
442 bioinformatics. Expression matrices then underwent normalization, scaling, principal
443 components analysis, and subsequent t-SNE analysis using Seurat packages. Seurat was then
444 used to generate conserved genes, differentially expressed genes, feature plots, dot plots, and
445 ridge plots. Cell clusters were then defined querying conserved genes and differentially
446 expressed genes against the Immgen gene expression database (www.immgen.org) using the
447 interactive tool "My Gene Set."
448
449 *Histology*
450 Biopsies from mouse skin tissue were removed and fixed in 4% paraformaldehyde overnight
451 and then transferred to 70% ethanol. Samples were then submitted to the Johns Hopkins
452 Oncology Tissue Services Core facility where they were embedded in paraffin. Tissue sections
453 were obtained at 4µm thickness and mounted onto glass slides, followed by hematoxylin and
454 eosin (H&E) staining.
455
456 *Immunofluorescence and immunohistochemistry*
457 Immunofluorescence microscopy was performed on de-paraffinized tissue sections that
458 received heat-induced antigen retrieval using Target Retrieval Solution (Agilent Dako, S169984-
459 2). After washing and permeabilization in TBS-T universal buffer (0.2% Triton X-100 in tris-
460 buffered saline), sections were blocked at room temperature in 5% goat, donkey, or fetal
461 bovine serum with 1% bovine serum albumin. Tissue sections were then incubated overnight at
462 4°C with primary antibodies (Extended Table 2) in Antibody Diluent (Agilent Dako, S080983-2).
463 Following a wash step, sections were incubated in fluorescent-dye conjugated secondary
464 antibodies diluted in antibody diluent for 1 hour at room temperature. After final washing,
465 sections were mounted with VECTASHIELD® Hardset™ Antifade Mounting Medium with DAPI
466 (Vector Laboratories, H-1500) for nuclear staining. All imaging was done on a DFC365FX (Leica)
467 at 20x and 40x magnifications.
468

469
470 *U1 in situ hybridization*
471 U1 in situ probes were designed and ordered in the Stellaris Probe Designer (Biosearch
472 Technologies) (Extended Table 3). Tissue sections were de-parafinized and stained following
473 Biosearch Technologies Stellaris RNA FISH protocol for Formalin-Fixed Paraffin-Embedded
474 Tissue. Briefly, tissue sections were washed in Wash Buffer A (Biosearch Technologies, SMF-
475 WA1-60), before adding 200µl hybridization buffer (Biosearch Technologies, SMF-HB1-10)
476 containing the U1 probe and covering the tissue with a glass coverslip. The slides were then
477 incubated overnight in a humid box at 37°C. Slides were then immersed in Wash Buffer A in the
478 dark at 37°C for 30 minutes, allowing the coverslips to float off. Slides were then washed for 5
479 minutes with Wash Buffer B (Biosearch Technologies, SMF-WB1-20), before sections were
480 mounted with VECTASHIELD® Hardset™ Antifade Mounting Medium with DAPI (Vector
481 Laboratories, H-1500) for nuclear staining. All imaging was done on a DFC365FX (Leica) at 63x
482 magnifications.
483
484 *Microarray, RNA-seq and proteomic analysis*
485 Proteins from the wound center and wound edges were analyzed by proteomics, as previously
486 described[37]. Briefly, we used Orbitrap Fusion Tribrid mass spectrometer (Thermo Scientific) for
487 protein profiling and obtained the protein expression level by the MS Amanda algorithm.
488 Standard bioinformatics procedures were performed, including standardization of gene
489 expression, the definition of differentially expressed genes, and GO enrichment analysis. For
490 both Rnasel-/- and WT mice, total RNA was isolated from mouse tissue at the time of scab
491 detachment from the wound (~10 days post-wounding). RNA was submitted to the JHMI Deep
492 Sequencing & Microarray core facility and profiled using the Affymetrix Clariom™ S mouse array
493 platform, according to the manufacturer's protocols. Gene chips were scanned, generating CEL
494 pixel intensity files, which were processed and analyzed using Partek® Genomics Suite™
495 software, and the Robust Multichip Analysis (RMA) algorithm was used for normalization.
496 For SPF and GF analysis, total RNA from early wound bed skin (~WD12) was submitted to the
497 JHMI Transcriptomics and Deep Sequencing Core. The 1.0ST exon sequencing of mouse RNA
498 was performed according to the manufacturer's standard protocol. The raw affymetrix CEL data
499 was standardized using Robust Multichip Analysis (RMA) algorithm for comparison.
500
501 *Quantification and Statistical Analysis*
502 All in vivo and in vitro experiments were performed in at least individual instances. Univariate
503 statistical analysis was performed using Student's t-test, and multivariate analysis was
504 performed using ANOVA. All statistical analyses and graphical representations were generated
505 using GraphPad Prism software. Statistical significance is defined as p-values <0.05 derived
506 from the standard error of mean calculations.
507
508
509 **Extended Table 1**

Name	Host	Fluorophore	Manufacturer/Product #

MHCII (IA/IE)	Rat	BV421/Pacific Blue	BioLegend/107631
CD3	Rat	BV510/AmCyan	BD/740147
Ly6C	Rat	FITC	BD/553104
Ly6G	Rat	PE	BioLegend/127607
CD45	Rat	PE-Cy5.5	Invitrogen/35-0451-82
CD115	Rat	PE-Vio770	BioLegend/135523
CD11c	Hamster	APC	BioLegend/117310
CD11b	Rat	APC-Cy7	BD/557657

510

511 **Extended Table 2**

Name	Host	Dilution	Company/ Product #
MPO	Goat	1:200	Abcam/ab208670
F4/80	Rat	1:200	Abcam/ab6640
Ly6G	Rat	1:200	BioXCell/BP0075-1
H3Cit	Rabbit	1:500	Abcam/ab5103
Alexa Fluor® 488 Anti-Goat IgG (H+L)	Rabbit	1:1000	Invitrogen/A27012
Alexa Fluor® 488 Anti-Rabbit Ig (H+L)	Goat	1:1000	Invitrogen/A-11008
Alexa Fluor® 594 Anti-Rabbit IgG (H+L)	Goat	1:1000	Invitrogen/A-11037

Alexa Fluor® 488 Anti-Rat Ig (H+L)	Goat	1:1000	Invitrogen/A-11006
Alexa Fluor® 594 Anti-Rat Ig (H+L)	Donkey	1:1000	Invitrogen/ A-21209

512
513 **Extended Table 3**

Sequence Name	Sequence
U1 snRNA_1	cccctgccaggtaagtat
U1 snRNA_2	caccttcgtgatcatggt
U1 snRNA_3	aagcctcgccctgggaaa
U1 snRNA_4	acatccggagtgcaatgg
U1 snRNA_5	gggaaatcgcaggggtca
U1 snRNA_6	cagtcgagtttcccacat
U1 snRNA_7	ccccactaccacaaatta
U1 snRNA_8	aggggaaagcgcgaacgc

514
515
516 **Figure Legends**
517
518 **Figure 1: Neutrophil signature correlates with high skin regeneration in multiple models**
519 **a.** Schematic of hair neogenesis preferential localization to wound center (high WIHN) rather
520 than wound edge (low WIHN). **b.** Proteomic gene ontology (GO) analysis of the top 100 genes
521 wound center versus wound edge in wild type mice (at scab detachment) shows a
522 predominance in innate immune response pathways and neutrophil signatures. **c.** Abundance
523 ratios of genes from select GO terms highlighted in b. show enrichment of antimicrobial and
524 granular proteins, labeled in red. **d.** GO analysis of the top 200 genes from high WIHN Rnasel$^{-/-}$
525 versus wild-type mice at scab detachment shows a predominance of neutrophil and innate
526 immune cell chemotaxis pathways. Inset graphs show the gene fold expression changes for
527 genes present in that category. **e.** Neutrophil chemotaxis and innate immune categories are
528 included in Gene Ontology (GO) enrichment analysis of the top versus bottom 500 differentially
529 expressed genes between Specific pathogen-free (SPF; high WIHN) and germ-free (GF; low
530 WIHN) mice on ~WD12 (scab detachment) wound beds. (n=3 independent animals per group).
531 Inset graphs show the gene fold expression changes for genes present in that category.
532
533

534 **Figure 2: Neutrophils persist in wound bed after the acute inflammatory phase, producing**
535 **extracellular traps**
536 **a.** Neutrophils are present in the wound beds of C57BL/6J mice at early time points, visible in
537 representative hematoxylin and eosin [H&E] staining. Red arrows show select neutrophils,
538 evident by their multilobular nuclei. The black dashed line signifies the migrating epithelial
539 front. Black scale bar = 50 µm. **b.** Neutrophils predominate throughout the wound beds of
540 C57BL/6J mice on wound days 1 and 3, visible in prominent MPO immunofluorescence (green).
541 Few macrophages are present (Red, F4/80). Red arrows show select neutrophils. The white
542 dashed line signifies the dorsal edge of the wound bed. White scale bar = 200 µm. **c.** Percent
543 neutrophil (Ly6G+ cells from total CD45+ cells) levels are consistent in the blood throughout the
544 wound time course, but drop in the wound bed at wound day 11, as measured by FACS. ****p
545 < 0.0001, as calculated by two-way ANOVA. n.s., not significant. N = 2 vs 4. Results are
546 representative of at least two independent experiments. **d.** Citrullinated histone H3 (H3Cit, red)
547 co-localized with Ly6G+ neutrophils (green), beginning at wound day 3 in the wound beds of
548 immunofluorescence stained C57BL/6J mice, indicating the formation of extracellular traps. Red
549 arrows show select neutrophils. The white dashed line signifies the dorsal edge of the wound
550 bed. White scale bar = 200 µm. **e.** Neutrophil extracellular trap positive cells (MPO+, SYTOX
551 green +) are present at late wound time points, but are absent in the wound beds of PAD4-/-
552 mice, as measured by FACs ****p < 0.0001, as calculated by two-way ANOVA. n.s., not
553 significant. N = 7 vs 4. Results are representative of at least two independent experiments. **f.**
554 Cytoplasmic U1 snRNA is present in the wound bed of C57BL/6J mice, while it localized
555 exclusively in the nuclei of unwounded controls, as visualized by representative FISH. White
556 arrows show select cells with nuclear or cytoplasmic U1 snRNA. The white dashed line signifies
557 the dorsal edge of the wound bed. The solid white line delineates a hair follicle. White scale bar
558 = 80 µm
559
560
561 **Figure 3: Large full-thickness wounds dramatically reduce antibody-mediated neutrophil**
562 **depletion**
563 **a.** Schematic of neutrophil depletion via intraperitoneal injection (IP) of Ly6G antibody (1A8
564 clone, 500µg), Gr1 (Ly6G/Ly6C, RB6-8C5 clone, 200ng), or isotype control. IP injections are done
565 one day before and one day after wounding C57BL/J6 mice with 1.25cm^2 square wounds. Mice
566 were then sacrificed wound day 2 or 2 for FACs analysis of blood or wound bed (WB). **b.**
567 Antibody mediated depletion is not successful in the wound bed. Representative flow plots
568 from the wound beds (wound day 3) of mice treated as in **a.** The percent neutrophils (CD11b+,
569 Ly6c+) present in these samples are presented to the right. The difference between samples is
570 statistically insignificant, as calculated by the two-tailed Student's t-test. N = 2. Results are
571 representative of at least two independent experiments. **c.** Antibody mediated. Neutrophil
572 depletion is marginally successful in the blood, but not the wound bed, two days after
573 wounding. The percent neutrophils (CD11b+, Ly6c+), at wound day 2, present in the blood and
574 wound beds of mice treated as in **a.** (Ly6G, 1A8). **p < 0.0011, as calculated by two-way
575 ANOVA. n.s., not significant. N = 4. Results are representative of at least two independent
576 experiments. **d.** Neutrophil depletion from the blood is successful 1-day post injection (Ly6G,
577 1A8), in the absence of wounding, via FACs. The neutrophil depletion is statistically significant.

578 ****p < 0.0001, as calculated by two-tailed Student's t-test. N = 4 vs 6. **e.** The efficacy of
579 neutrophil depletion from the blood diminishes after 1.25X1.25cm^2 wounds are inflicted. The
580 percent neutrophils (Gr1+, Ly6c+) in the blood at wound day 2, via FACs. The neutrophil
581 depletion is statistically insignificant. n.s., not significant. N = 2 vs 3. Results are representative
582 of at least three independent experiments. **f.** Neutrophil depletion from the blood is more
583 pronounced in unwounded mice. The percent neutrophils (Gr1+, Ly6c+) present in the blood at
584 wound day 2 of mice IP injected with Ly6G antibody (1A8, 500 µg), with or without wounding,
585 via FACs. ****p < 0.0001 vs **p=0.0038 as calculated by two-way ANOVA. N = 6 vs 7. **g.**
586 Neutrophil depletion from the skin is ineffective, regardless of wound status. The percent
587 neutrophils (Gr1+, Ly6c+) present in the wound bed or skin at wound day 2 of mice IP injected
588 with Ly6G antibody (1A8, 500ug), with or without wounding. The neutrophil depletion is
589 insignificant in both cases, as calculated by two-way ANOVA. n.s., not significant. N = 6 vs 7. **h.**
590 C57BL/6J mice were given full thickness wounds on the center of their backs. The normal large
591 wound (LW) is 1.25x1.25cm^2, while the smaller wound (SW) is 0.6x0.6cm^2. **i.** Neutrophil
592 depletion from the blood is successful on small, but not large wounded mice. Mice wounded
593 with small or large wounds (**h.**) were IP injected with Ly6G antibody (1A8, 500µg) one day
594 before and after wounding. Blood was extracted on wound day 2 and analyzed by flow
595 cytometry for percent neutrophils (Gr1+, Ly6c+). *p = 0.0362 as calculated by two-way ANOVA.
596 n.s., not significant. N = 2 vs 3 and 2 vs 2. Results are representative of at least two independent
597 experiments. **j.** Neutrophil depletion from the wound bed is successful on small, but not large
598 wounded mice. Mice wounded with small or large wounds (**h.**) were IP injected with Ly6G
599 antibody (1A8, 500µg) one day before and after wounding. Wound beds were collected on
600 wound day 2 and analyzed by flow cytometry for percent neutrophils (Gr1+, Ly6c+). Depletion
601 was significant in the small wound, but not the large wound setting. *p = 0.0458 as calculated
602 by two-way ANOVA. n.s., not significant. N = 2 vs 3 and 2 vs 2. Results are representative of at
603 least two independent experiments.
604
605
606 **Figure 4: Mature neutrophils inhibit wound induced hair neogenesis**
607 **a.** Schematic of neutrophil depletion via IP of Ly6G antibody (100µg) or isotype control. IP
608 injections are done one day before and one day after wounding C57BL/J6 mice with
609 1.25x1.25cm^2 square wounds. Wound induced hair neogenesis (WIHN) was measured 21 days
610 after wounding via confocal scanning laser microscopy (CSLM). **b.** Neutrophil targeted Ly6G
611 antibody injected mice exhibit increased WIHN (CSLM, images; fold = 3.94, p = 0.011, N = 10 vs
612 9). In each image, the dash red box indicates the area of hair follicle regeneration. **c.** Diphtheria
613 toxin (DT, 250ng) injection in heterozygous ROSA26iDTR/MRP8-Cre-ires mice (PMN^{DTR} and
614 PMN^{WT}), following the injection scheme in **a.**, successfully depletes neutrophils from the blood
615 in mice with large wounds**.** Fold = -4.33. **p = 0.0098. N = 2 vs. 3. Results are representative of
616 at least two independent experiments. **d.** Mice treated as in **c.** are depleted of neutrophils in
617 their wound beds at wound day 2. Fold = -4.27. **p = 0.0069. N = 2 vs. 3. Results are
618 representative of at least two independent experiments. **e.** PMN^{DTR} mice IP injected with
619 diphtheria toxin (DT, 250ng) on wound days -1 and 1 exhibit increased WIHN (CSLM, images;
620 fold = 3.23, ***p = 0.0010, N = 14 vs 6). In each image, the dash red box indicates the area of
621 hair follicle regeneration. **f.** Regenerated hair follicles after the injection of 50k-200k purified

622 neutrophils underneath the scab at WD7-8. (CSLM, images; n.s., not significant, N = 9 vs 3 vs 6).
623 In each image, the dash red box indicates the area of hair follicle regeneration. **g.** Pad4$^{-/-}$ mice
624 defective in extracellular traps exhibit increased WIHN (CSLM, images; fold = 2.47, p = 0.026, N
625 = 10 vs 19). In each image, the dash red box indicates the area of hair follicle regeneration. **h.**
626 Tlr3$^{-/-}$ mice exhibit decreased WIHN (fold = -3.75 p = 0.0218, N = 8 vs 10). **i.** The presence of
627 increased neutrophils correlates with decreased WIHN in TLR3$^{-/-}$ mice. scRNA-seq t-SNE plot
628 shows differences between WT (red, 4150 cells) and Tlr3-/- (blue, 5648 cells) wound beds at
629 wound day 10. The plots were generated via Seurat. The neutrophil cluster is circled in red.
630 Percent of neutrophils are graphed to the right. **j.** Neutrophil associated gene expression is
631 more pronounced within the neutrophils of Tlr3-/- mice, compared to WT. Generated in Seurat
632 with RidgePlot function.
633
634 **Supplementary Figure Legends**
635
636 **S1:** Macrophage (F4/80) levels are largely absent from the blood and low in the wound bed
637 during the early phase of healing, but increase dramatically at wound day 11, as measured by
638 FACS. ***p < 0.004, as calculated by two-way ANOVA. n.s., not significant. N = 2 vs 4. Results
639 are representative of at least two independent experiments.
640
641 **S2:** Ly6G 1A8 antibody clone (Bio-X-Cell) masks the Ly6G epitope, preventing detection by the
642 Ly6G REA526 clone (Miltenyi, engineered 1A8 clone) and partially preventing detection by the
643 Gr1 RB6-8C5 clone (Bio-X-Cell) antibodies. Blood was extracted from a single C57BL/6J and
644 stained sequentially with combinations of two antibodies, to test Ly6G epitope masking, before
645 detecting by flow cytometry. If only stained with the Ly6G (REA526) or Gr1 (RB6-8C5), the
646 neutrophil population is detected normally (13.7% or 13.2%, respectively). If you first stain with
647 Ly6G (1A8 clone), followed by Ly6G (REA526) or Gr1 (RB6-8C5), you get varying degrees of Ly6G
648 antibody masking. Being a derivative of the 1A8 clone, the REA526 Ly6G binding site is almost
649 completely blocked by the prior incubation with the Ly6G 1A8 clone (1.10%), making the pair
650 unusable for neutrophil depletion experiments. Prior incubation with the Ly6G 1A8 clone
651 followed by Gr1 (recognized an epitope of Ly6G/Ly6C) shifts the neutrophil population to the
652 left, but they remain distinct from the negatively stained cells (12.7%). With careful gating, this
653 makes depletion with the Ly6G (1A8 clone) antibody and detection with the Gr1 (RB6-8C5)
654 antibody possible. The neutrophil population is boxed in red.
655
656 **S3:** Antibody mediated Neutrophil depletion is not efficient in the blood, spleen, liver, or wound
657 bed, two days after wounding. The percent neutrophils (CD11b+, Ly6c+), at wound day 2,
658 present in the blood, spleen, liver, and wound beds of mice IP injected with Ly6G antibody
659 (500µ, 1A8) one day before and one day after given 1.25x1.25cm^2 full thickness wounds. The
660 neutrophil depletion is statistically insignificant, as calculated by two-way ANOVA. n.s., not
661 significant. N = 4 vs 4, except for the Blood and Wound bed samples, which were 7 vs. 7.
662
663 **S4:** The wound closure rate was not affected by neutrophil depletion via IP of Ly6G antibody
664 (100µg) or isotype control. IP injections were done one day before and one day after wounding

C57BL/J6 mice with 1.25x1.25cm^2 square wounds. N = 4 vs 4. Results are representative of three independent experiments.

S5. PMN^{DTR} mice IP injected with diphtheria toxin (DT, 250ng) on wound days 6, 8, and 10 exhibit increased WIHN (CSLM, images; fold = 3.28, **p = 0.0085, N = 13 vs 5).

S6: a. Schematic of neutrophil depletion via IP of Ly6G antibody (500µg) or isotype control. IP injections are done on wound day 8 and 10, after wounding C57BL/J6 mice with 1.25x1.25cm^2 square wounds. Wound induced hair neogenesis (WIHN) was measured 21 days after wounding via confocal scanning laser microscopy (CSLM). **b.** Neutrophil depletion in the blood is successful on wound day 9, one day after antibody injection (Ly6G, 1A8), via FACs. The neutrophil depletion is statistically significant. ****p < 0.0001, as calculated by two-tailed Student's t-test. Fold = -87.9. N = 2 vs 3. **c.** Late stage Ly6G antibody injected mice exhibit normal WIHN (CSLM, images; n.s., not significant, N = 3 vs 3). In each image, the dash red box indicates the area of hair follicle regeneration.

S7: a. Tlr3$^{-/-}$ mice exhibit decreased WIHN (representative CSLM images, N = 8 vs. 10). In each image, the dash red box indicates the area of hair follicle regeneration. **b.** Neutrophil associated genes used to identify the neutrophil cluster in UMAP non-linear dimensional reduction, via Seurat R package, of WT and Tlr3-/- mice.

Works Cited:

1. Diegelmann, R.F. & Evans, M.C. Wound healing: an overview of acute, fibrotic and delayed healing. *Frontiers in bioscience : a journal and virtual library* **9**, 283-289 (2004).
2. O'Connell, J.B. The economic burden of heart failure. *Clinical cardiology* **23**, III6-10 (2000).
3. Chung, F.*, et al.* Assessing the burden of respiratory disease in the UK. *Respiratory medicine* **96**, 963-975 (2002).
4. Godwin, J.W., Pinto, A.R. & Rosenthal, N.A. Macrophages are required for adult salamander limb regeneration. *Proceedings of the National Academy of Sciences of the United States of America* **110**, 9415-9420 (2013).
5. Kyritsis, N.*, et al.* Acute inflammation initiates the regenerative response in the adult zebrafish brain. *Science* **338**, 1353-1356 (2012).
6. Taniguchi, K.*, et al.* A gp130-Src-YAP module links inflammation to epithelial regeneration. *Nature* **519**, 57-62 (2015).
7. Gay, D.*, et al.* Fgf9 from dermal gammadelta T cells induces hair follicle neogenesis after wounding. *Nature medicine* **19**, 916-923 (2013).

706 8. Kasuya, A., Ito, T. & Tokura, Y. M2 macrophages promote wound-induced hair
707 neogenesis. *Journal of dermatological science* **91**, 250-255 (2018).
708 9. Rahmani, W.*, et al.* Macrophages Promote Wound-Induced Hair Follicle Regeneration in
709 a CX3CR1- and TGF-beta1-Dependent Manner. *The Journal of investigative dermatology*
710 **138**, 2111-2122 (2018).
711 10. Wang, X.*, et al.* Macrophages induce AKT/beta-catenin-dependent Lgr5(+) stem cell
712 activation and hair follicle regeneration through TNF. *Nature communications* **8**, 14091
713 (2017).
714 11. Seifert, A.W.*, et al.* Skin shedding and tissue regeneration in African spiny mice
715 (Acomys). *Nature* **489**, 561-565 (2012).
716 12. Billingham, R.E. & Russell, P.S. Incomplete wound contracture and the phenomenon of
717 hair neogenesis in rabbits' skin. *Nature* **177**, 791-792 (1956).
718 13. Breedis, C. Regeneration of hair follicles and sebaceous glands from the epithelium of
719 scars in the rabbit. *Cancer research* **14**, 575-579 (1954).
720 14. Kligman, A.M. & Strauss, J.S. The formation of vellus hair follicles from human adult
721 epidermis. *The Journal of investigative dermatology* **27**, 19-23 (1956).
722 15. Lacassagne, A. & Latarjet, R. Action of methylcholanthrene on certain scars of the skin in
723 mice. *Cancer research* **6**, 183-188 (1946).
724 16. Ito, M.*, et al.* Wnt-dependent de novo hair follicle regeneration in adult mouse skin after
725 wounding. *Nature* **447**, 316-320 (2007).
726 17. Plikus, M.V.*, et al.* Regeneration of fat cells from myofibroblasts during wound healing.
727 *Science* **355**, 748-752 (2017).
728 18. Kim, M.H.*, et al.* Dynamics of neutrophil infiltration during cutaneous wound healing
729 and infection using fluorescence imaging. *The Journal of investigative dermatology* **128**,
730 1812-1820 (2008).
731 19. Guo, S. & Dipietro, L.A. Factors affecting wound healing. *Journal of dental research* **89**,
732 219-229 (2010).
733 20. Segal, A.W. How neutrophils kill microbes. *Annual review of immunology* **23**, 197-223
734 (2005).
735 21. Brinkmann, V.*, et al.* Neutrophil extracellular traps kill bacteria. *Science* **303**, 1532-1535
736 (2004).
737 22. Papayannopoulos, V. Neutrophil extracellular traps in immunity and disease. *Nature*
738 *reviews. Immunology* **18**, 134-147 (2018).
739 23. Acosta, J.B.*, et al.* The pro-inflammatory environment in recalcitrant diabetic foot
740 wounds. *International wound journal* **5**, 530-539 (2008).
741 24. Singer, A.J. & Clark, R.A. Cutaneous wound healing. *The New England journal of*
742 *medicine* **341**, 738-746 (1999).
743 25. DiPietro, L.A. Wound healing: the role of the macrophage and other immune cells. *Shock*
744 **4**, 233-240 (1995).
745 26. Takeuchi, O. & Akira, S. Pattern recognition receptors and inflammation. *Cell* **140**, 805-
746 820 (2010).
747 27. Huebener, P. & Schwabe, R.F. Regulation of wound healing and organ fibrosis by toll-like
748 receptors. *Biochimica et biophysica acta* **1832**, 1005-1017 (2013).

749 28. Kawai, T. & Akira, S. Toll-like receptor and RIG-I-like receptor signaling. *Annals of the*
750 *New York Academy of Sciences* **1143**, 1-20 (2008).
751 29. Cavassani, K.A.*, et al.* TLR3 is an endogenous sensor of tissue necrosis during acute
752 inflammatory events. *The Journal of experimental medicine* **205**, 2609-2621 (2008).
753 30. Lin, Q.*, et al.* Impaired wound healing with defective expression of chemokines and
754 recruitment of myeloid cells in TLR3-deficient mice. *Journal of immunology* **186**, 3710-
755 3717 (2011).
756 31. Lin, Q.*, et al.* Toll-like receptor 3 ligand polyinosinic:polycytidylic acid promotes wound
757 healing in human and murine skin. *The Journal of investigative dermatology* **132**, 2085-
758 2092 (2012).
759 32. Bernard, J.J.*, et al.* Ultraviolet radiation damages self noncoding RNA and is detected by
760 TLR3. *Nature medicine* **18**, 1286-1290 (2012).
761 33. Borkowski, A.W.*, et al.* Toll-like receptor 3 activation is required for normal skin barrier
762 repair following UV damage. *The Journal of investigative dermatology* **135**, 569-578
763 (2015).
764 34. Nelson, A.M.*, et al.* dsRNA Released by Tissue Damage Activates TLR3 to Drive Skin
765 Regeneration. *Cell stem cell* **17**, 139-151 (2015).
766 35. Zhu, A.S., Li, A., Ratliff, T.S., Melsom, M. & Garza, L.A. After Skin Wounding, Noncoding
767 dsRNA Coordinates Prostaglandins and Wnts to Promote Regeneration. *The Journal of*
768 *investigative dermatology* **137**, 1562-1568 (2017).
769 36. Lai, Y.*, et al.* Commensal bacteria regulate Toll-like receptor 3-dependent inflammation
770 after skin injury. *Nature medicine* **15**, 1377-1382 (2009).
771 37. Kim, D.*, et al.* Noncoding dsRNA induces retinoic acid synthesis to stimulate hair follicle
772 regeneration via TLR3. *Nature communications* **10**, 2811 (2019).
773 38. Liu, Y.*, et al.* Tumor Exosomal RNAs Promote Lung Pre-metastatic Niche Formation by
774 Activating Alveolar Epithelial TLR3 to Recruit Neutrophils. *Cancer cell* **30**, 243-256
775 (2016).
776 39. Zhang, L.J.*, et al.* Antimicrobial Peptide LL37 and MAVS Signaling Drive Interferon-beta
777 Production by Epidermal Keratinocytes during Skin Injury. *Immunity* **45**, 119-130 (2016).
778 40. Chow, O.A.*, et al.* Statins enhance formation of phagocyte extracellular traps. *Cell host &*
779 *microbe* **8**, 445-454 (2010).
780 41. Mohanan, S., Horibata, S., McElwee, J.L., Dannenberg, A.J. & Coonrod, S.A. Identification
781 of macrophage extracellular trap-like structures in mammary gland adipose tissue: a
782 preliminary study. *Frontiers in immunology* **4**, 67 (2013).
783 42. Boe, D.M., Curtis, B.J., Chen, M.M., Ippolito, J.A. & Kovacs, E.J. Extracellular traps and
784 macrophages: new roles for the versatile phagocyte. *Journal of leukocyte biology* **97**,
785 1023-1035 (2015).
786 43. Rossaint, J.*, et al.* Synchronized integrin engagement and chemokine activation is crucial
787 in neutrophil extracellular trap-mediated sterile inflammation. *Blood* **123**, 2573-2584
788 (2014).
789 44. Maugeri, N.*, et al.* Activated platelets present high mobility group box 1 to neutrophils,
790 inducing autophagy and promoting the extrusion of neutrophil extracellular traps.
791 *Journal of thrombosis and haemostasis : JTH* **12**, 2074-2088 (2014).

792 45. Keshari, R.S.*, et al.* Cytokines induced neutrophil extracellular traps formation:
793 implication for the inflammatory disease condition. *PloS one* **7**, e48111 (2012).
794 46. Gupta, A.K., Giaglis, S., Hasler, P. & Hahn, S. Efficient neutrophil extracellular trap
795 induction requires mobilization of both intracellular and extracellular calcium pools and
796 is modulated by cyclosporine A. *PloS one* **9**, e97088 (2014).
797 47. Wong, K.W. & Jacobs, W.R., Jr. Mycobacterium tuberculosis exploits human interferon
798 gamma to stimulate macrophage extracellular trap formation and necrosis. *The Journal*
799 *of infectious diseases* **208**, 109-119 (2013).
800 48. Wong, S.L.*, et al.* Diabetes primes neutrophils to undergo NETosis, which impairs wound
801 healing. *Nature medicine* **21**, 815-819 (2015).
802 49. Delgado-Rizo, V.*, et al.* Neutrophil Extracellular Traps and Its Implications in
803 Inflammation: An Overview. *Frontiers in immunology* **8**, 81 (2017).
804 50. Wang, Y.*, et al.* Histone hypercitrullination mediates chromatin decondensation and
805 neutrophil extracellular trap formation. *The Journal of cell biology* **184**, 205-213 (2009).
806 51. Wang, Y.*, et al.* Human PAD4 regulates histone arginine methylation levels via
807 demethylimination. *Science* **306**, 279-283 (2004).
808 52. Daley, J.M., Thomay, A.A., Connolly, M.D., Reichner, J.S. & Albina, J.E. Use of Ly6G-
809 specific monoclonal antibody to deplete neutrophils in mice. *Journal of leukocyte*
810 *biology* **83**, 64-70 (2008).
811 53. Ribechini, E., Leenen, P.J. & Lutz, M.B. Gr-1 antibody induces STAT signaling,
812 macrophage marker expression and abrogation of myeloid-derived suppressor cell
813 activity in BM cells. *European journal of immunology* **39**, 3538-3551 (2009).
814 54. Carr, K.D.*, et al.* Specific depletion reveals a novel role for neutrophil-mediated
815 protection in the liver during Listeria monocytogenes infection. *European journal of*
816 *immunology* **41**, 2666-2676 (2011).
817 55. Dovi, J.V., He, L.K. & DiPietro, L.A. Accelerated wound closure in neutrophil-depleted
818 mice. *Journal of leukocyte biology* **73**, 448-455 (2003).
819 56. Fan, C.*, et al.* Characterization and quantification of wound-induced hair follicle
820 neogenesis using in vivo confocal scanning laser microscopy. *Skin research and*
821 *technology : official journal of International Society for Bioengineering and the Skin* **17**,
822 387-397 (2011).
823 57. Reber, L.L.*, et al.* Neutrophil myeloperoxidase diminishes the toxic effects and mortality
824 induced by lipopolysaccharide. *The Journal of experimental medicine* **214**, 1249-1258
825 (2017).
826 58. Passegue, E., Wagner, E.F. & Weissman, I.L. JunB deficiency leads to a myeloproliferative
827 disorder arising from hematopoietic stem cells. *Cell* **119**, 431-443 (2004).
828 59. Elliott, E.R.*, et al.* Deletion of Syk in neutrophils prevents immune complex arthritis.
829 *Journal of immunology* **187**, 4319-4330 (2011).
830 60. Abram, C.L., Roberge, G.L., Pao, L.I., Neel, B.G. & Lowell, C.A. Distinct roles for
831 neutrophils and dendritic cells in inflammation and autoimmunity in motheaten mice.
832 *Immunity* **38**, 489-501 (2013).
833 61. Buch, T.*, et al.* A Cre-inducible diphtheria toxin receptor mediates cell lineage ablation
834 after toxin administration. *Nature methods* **2**, 419-426 (2005).

835 62. Kessenbrock, K.*, et al.* Netting neutrophils in autoimmune small-vessel vasculitis. *Nature*
836 *medicine* **15**, 623-625 (2009).
837 63. Hakkim, A.*, et al.* Impairment of neutrophil extracellular trap degradation is associated
838 with lupus nephritis. *Proceedings of the National Academy of Sciences of the United*
839 *States of America* **107**, 9813-9818 (2010).
840 64. Lande, R.*, et al.* Neutrophils activate plasmacytoid dendritic cells by releasing self-DNA-
841 peptide complexes in systemic lupus erythematosus. *Science translational medicine* **3**,
842 73ra19 (2011).
843 65. Garcia-Romo, G.S.*, et al.* Netting neutrophils are major inducers of type I IFN production
844 in pediatric systemic lupus erythematosus. *Science translational medicine* **3**, 73ra20
845 (2011).
846 66. Villanueva, E.*, et al.* Netting neutrophils induce endothelial damage, infiltrate tissues,
847 and expose immunostimulatory molecules in systemic lupus erythematosus. *Journal of*
848 *immunology* **187**, 538-552 (2011).
849 67. Leffler, J.*, et al.* Neutrophil extracellular traps that are not degraded in systemic lupus
850 erythematosus activate complement exacerbating the disease. *Journal of immunology*
851 **188**, 3522-3531 (2012).
852 68. Khandpur, R.*, et al.* NETs are a source of citrullinated autoantigens and stimulate
853 inflammatory responses in rheumatoid arthritis. *Science translational medicine* **5**,
854 178ra140 (2013).
855 69. Hu, S.C.*, et al.* Neutrophil extracellular trap formation is increased in psoriasis and
856 induces human beta-defensin-2 production in epidermal keratinocytes. *Scientific reports*
857 **6**, 31119 (2016).
858 70. Gan, T.*, et al.* TLR3 Regulated Poly I:C-Induced Neutrophil Extracellular Traps and Acute
859 Lung Injury Partly Through p38 MAP Kinase. *Frontiers in microbiology* **9**, 3174 (2018).
860 71. Liu, Q.*, et al.* Toll-Like Receptor 3 Signaling Contributes to Regional Neutrophil
861 Recruitment in Cultured Human Glomerular Endothelial Cells. *Nephron* **139**, 349-358
862 (2018).
863 72. Satija, R., Farrell, J.A., Gennert, D., Schier, A.F. & Regev, A. Spatial reconstruction of
864 single-cell gene expression data. *Nature biotechnology* **33**, 495-502 (2015).
865 73. Jiang, T.X., Harn, H.I., Ou, K.L., Lei, M. & Chuong, C.M. Comparative regenerative biology
866 of spiny (Acomys cahirinus) and laboratory (Mus musculus) mouse skin. *Exp Dermatol*
867 **28**, 442-449 (2019).
868 74. Brant, J.O., Yoon, J.H., Polvadore, T., Barbazuk, W.B. & Maden, M. Cellular events during
869 scar-free skin regeneration in the spiny mouse, Acomys. *Wound Repair Regen* **24**, 75-88
870 (2016).
871 75. Trujillo, G.*, et al.* Neutrophil recruitment to the lung in both C5a- and CXCL1-induced
872 alveolitis is impaired in vitamin D-binding protein-deficient mice. *Journal of immunology*
873 **191**, 848-856 (2013).
874 76. Metzemaekers, M., Gouwy, M. & Proost, P. Neutrophil chemoattractant receptors in
875 health and disease: double-edged swords. *Cell Mol Immunol* **17**, 433-450 (2020).
876 77. Lim, C.H.*, et al.* Hedgehog stimulates hair follicle neogenesis by creating inductive
877 dermis during murine skin wound healing. *Nature communications* **9**, 4903 (2018).

878 78. Kim, S.*, et al.* Simple cell culture media expansion of primary mouse keratinocytes.
879 *Journal of dermatological science* **93**, 135-138 (2019).
880

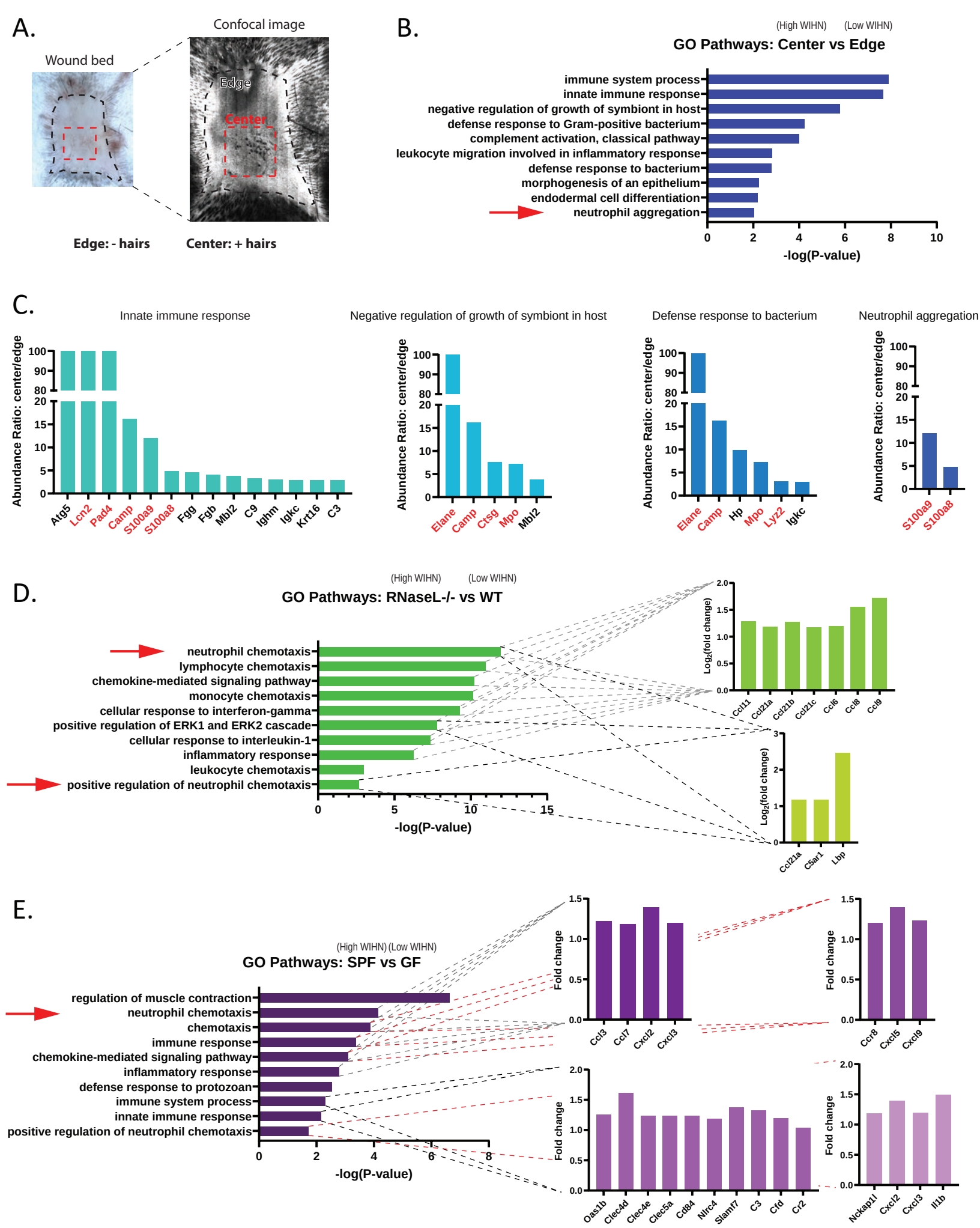

Figure 1: Neutrophil signature correlates with high skin regeneration in multiple models

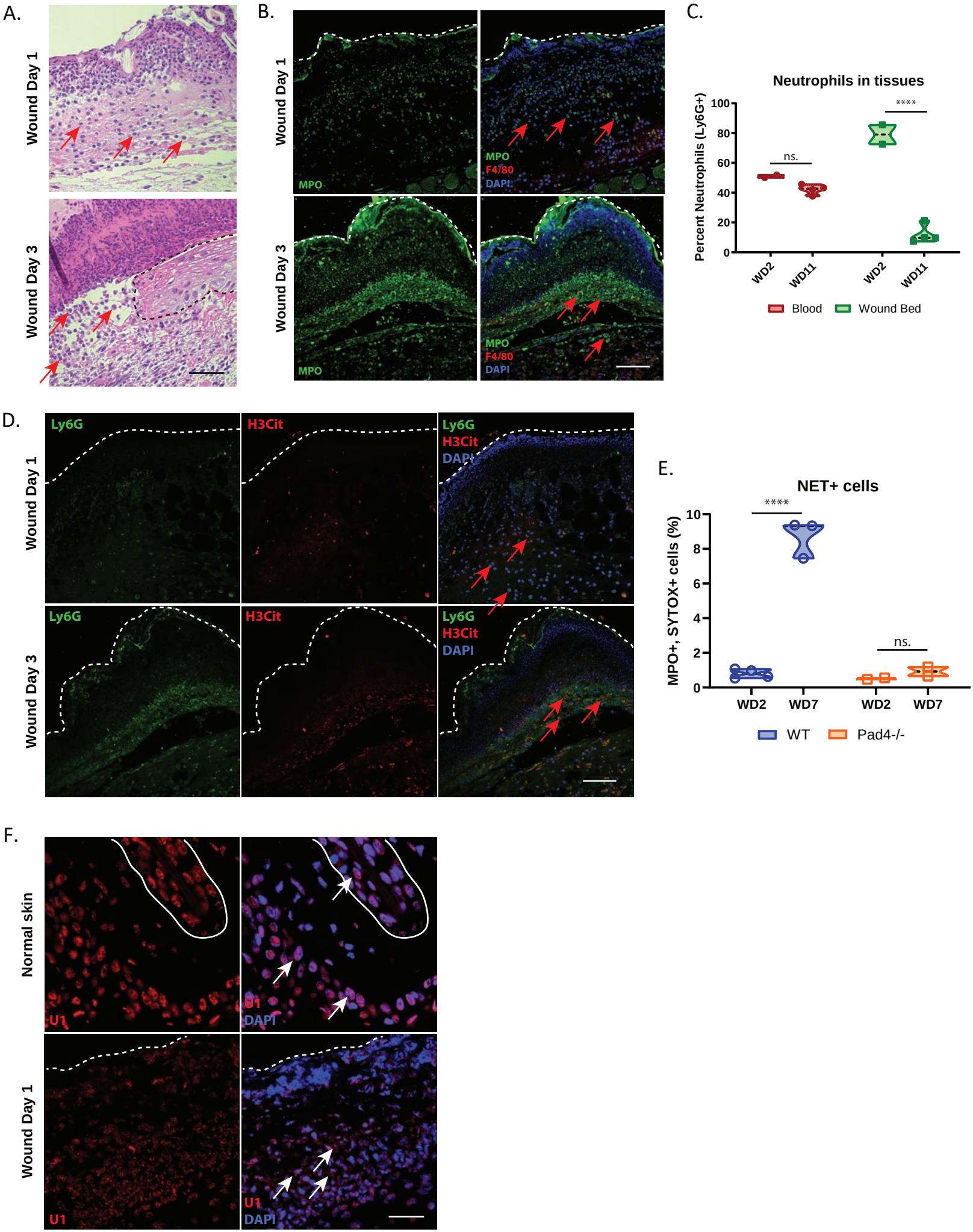

Figure 2: Neutrophils persist in wound bed after the acute inflammatory phase, producing extracellular traps

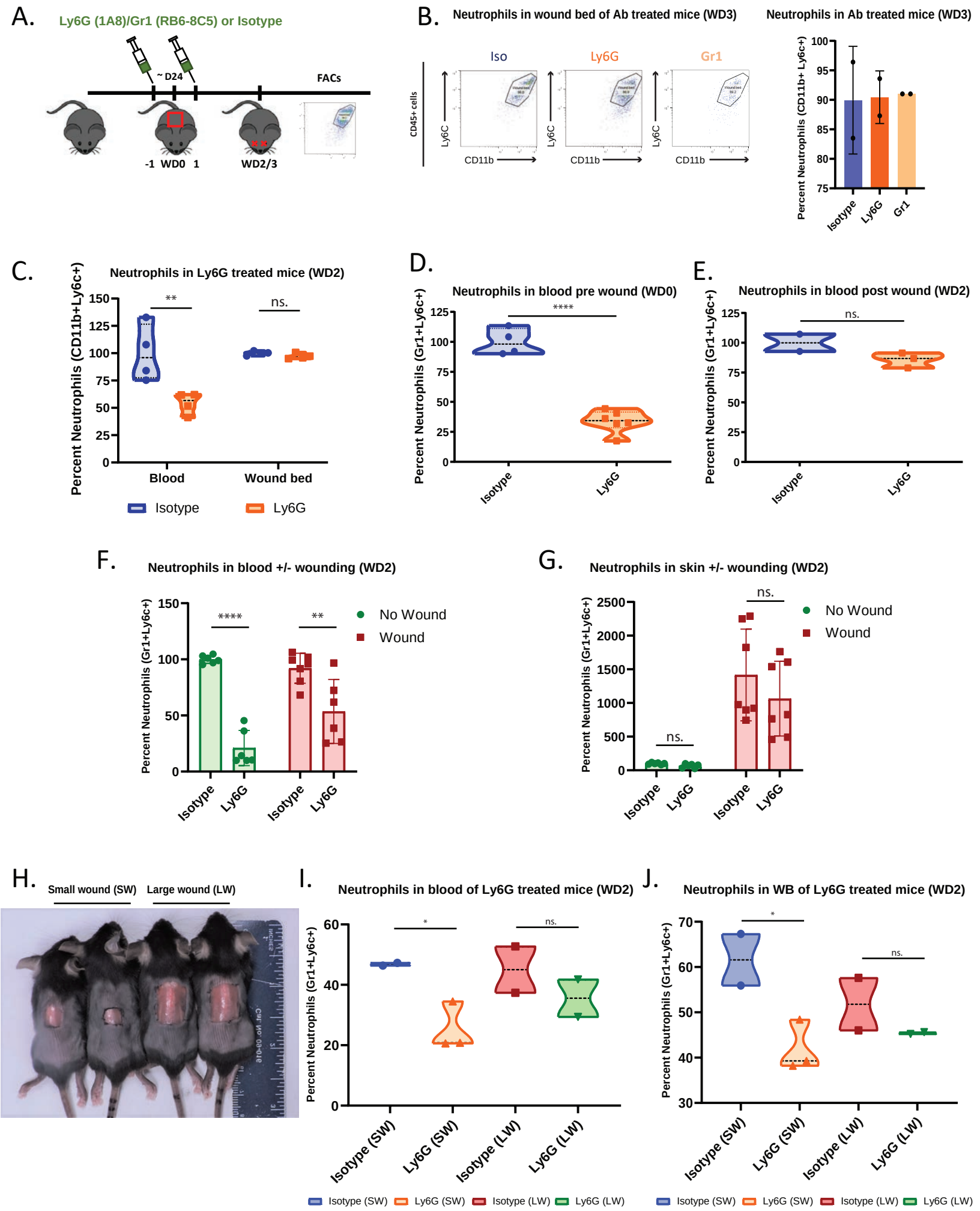

Figure 3: Large full-thickness wounds dramatically reduce antibody-mediated neutrophil depletion

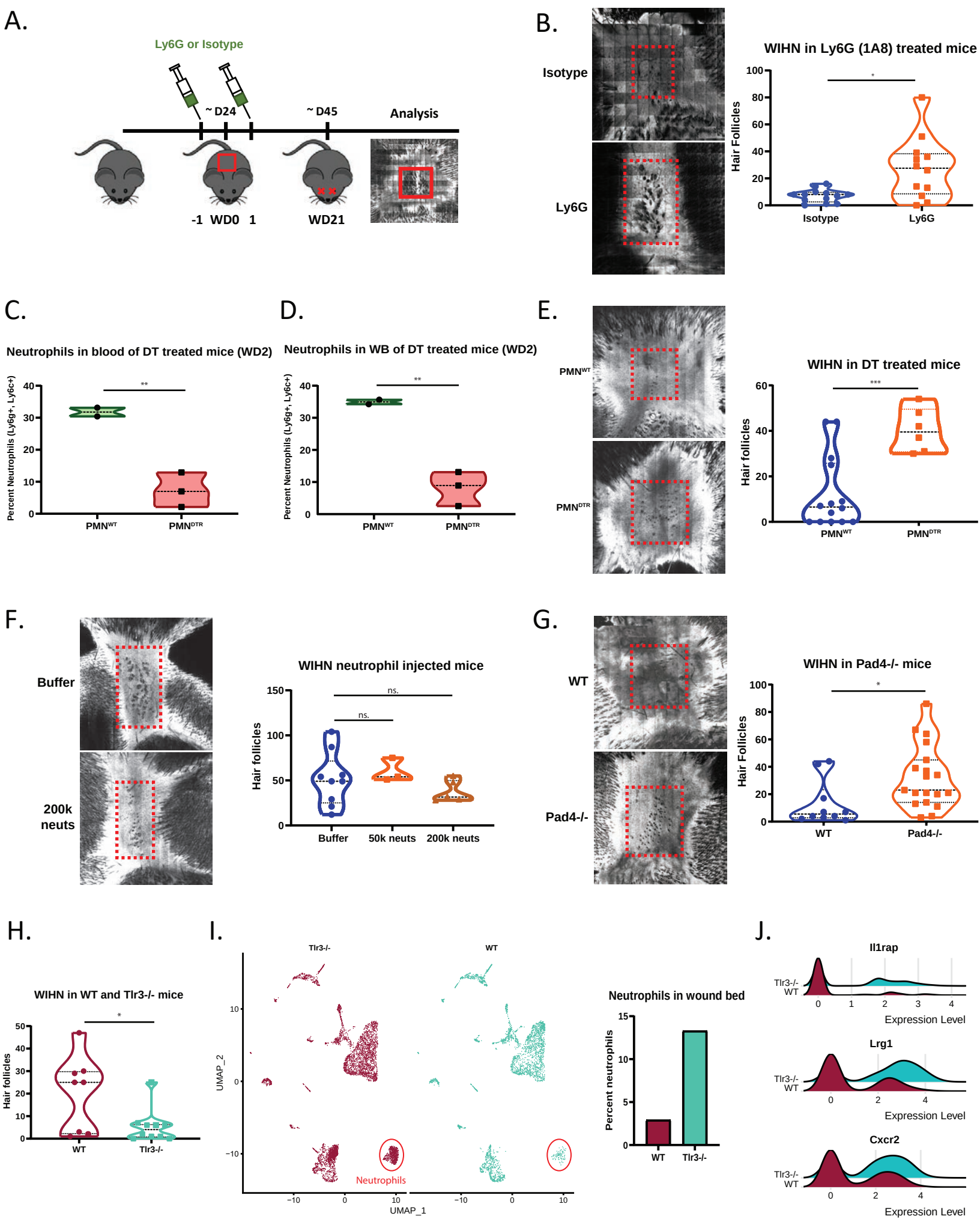

Figure 4: Neutrophils inhibit wound induced hair neogenesis